HHS Public Access

Author manuscript

Proc SPIE Int Soc Opt Eng. Author manuscript; available in PMC 2022 April 19.

Published in final edited form as:

Proc SPIE Int Soc Opt Eng. 2022 ; 11942: . doi:10.1117/12.2608288.

Evaluating interproximal and occlusal lesion severity with a dual SWIR transillumination/reflectance probe

Yihua Zhu, **Daniel Fried**

University of California, San Francisco, San Francisco, CA 94143-0758

Abstract

We have developed a clinical probe capable of acquiring simultaneous, multispectral short wavelength infrared (SWIR) reflectance and occlusal transillumination images of lesions on tooth proximal and occlusal surfaces to reduce the potential of false positives and enhance diagnosis. The dual probe was 3D printed and the imaging system uses an InGaAs camera and broadband light sources at 1310 nm for occlusal transillumination and 1600 nm for cross-polarization reflectance measurements. In this study a mathematical model to estimate the penetration depth of "hidden" occlusal lesions from the SWIR images was developed. We compared the model's estimated lesion depth on 18 extracted teeth with lesions against microCT measurements. Although the model estimated depth deviates from that measured in microCT at higher depths, there is a good linear correlation (R^2 = 0.93) between the estimated depth from SWIR images and the measured depth using microCT. SWIR occlusal transillumination images at 1300 nm also provide information about interproximal lesion penetration depth which can be directly viewed from the occlusal surface. SWIR occlusal transillumination and reflectance depth measurements on 49 natural interproximal lesions were compared with microCT measurements. There was significant correlation between the depths measured with SWIR occlusal transillumination (R^2 = 0.81) and reflectance (R^2 = 0.19) compared with the depths measured with microCT.

Keywords

SWIR imaging; dental caries; occlusal lesions; interproximal lesions

1. INTRODUCTION

Short wavelength infrared (SWIR) and near-IR (NIR) imaging methods have been under development for almost 20 years for use in dentistry and several clinical devices are now available commercially [1–5]. Due to the high transparency of enamel at SWIR wavelengths, novel imaging configurations are feasible in which the tooth can be imaged from the occlusal surface after shining light at and below the gum line, which we call occlusal transillumination [3, 6]. Interproximal lesions can be imaged by occlusal transillumination of the proximal contact points between teeth and by directing SWIR light below the crown while imaging the occlusal surface [6–8]. The latter approach is capable of imaging occlusal lesions as well with high contrast [2, 3, 6, 9–11]. In 2010, it was demonstrated that interproximal lesions that appeared on radiographs could be detected *in vivo* with SWIR imaging with similar sensitivity [6] and that occlusal transillumination could be employed clinically. This was the first step in demonstrating the clinical potential of SWIR/NIR

imaging for caries detection. In another clinical study at wavelengths greater than 1300 nm [12], we demonstrated that the sensitivity of SWIR imaging for interproximal and occlusal lesions was greater than radiographs. More recently we have combined SWIR reflectance and occlusal transillumination measurements taken at SWIR wavelengths into a single probe to reduce false positives since it is unlikely that confounding structural features or specular reflection (glare) are going to be present in both reflectance and transillumination images [10, 13–17].

We are also interested in developing improved methods of analysis to extract lesion depth and severity data from SWIR images. Our previous studies comparing the lesion contrast and the lesion depth have not shown a strong correlation with lesion contrast and severity [17]. Simon showed a positive correlation between the contrast with SWIR reflectance and the lesion depth for shallow occlusal lesions [14]. In addition, he demonstrated that the width of occlusal lesions in SWIR images correlated with the lesion depth [14]. In this paper, we compare the depth of lesions estimated using the dual occlusal transillumination and reflectance system operating at 1300 and 1600 nm with lesion depth and width data measured on extracted teeth with occlusal and interproximal lesions using microcomputed tomography (microCT). In addition, we introduce a simple model for estimating the depth of subsurface demineralization from the occlusal surface by comparing the contrast of surface and subsurface demineralization in reflectance measurements at 1600 nm. Most lesions of interest are located in the pits and fissures of the occlusal surface and at the proximal contact points in between teeth. Occlusal lesions that penetrate through the pits and fissures of the enamel can spread laterally in the soft underlying dentin. Often these lesions are not visible on radiographs even though they have spread extensively into the underlying dentin and they are called “hidden” lesions or questionable occlusal caries “QOCS”. The occlusal lesions are clearly visible where they reach the tooth surface at in the pits and fissures. The subsurface spread of occlusal lesions is also visible with optical coherence tomography (OCT), occlusal transillumination and reflectance at SWIR wavelengths due to the high transparency of enamel, however the contrast is lower since these lesion areas are located well below the surface under sound enamel [18, 19]. Interproximal lesions occur on the proximal contact points in between teeth and can also be seen from the occlusal surface through sound enamel even though they are located a few mm below the surface [6, 20, 21]. We have derived a simple mathematical model for estimating the depth of subsurface lesions using the Beer-Lambert law. This model requires the presence of demineralization located both below the surface and on the surface which is typical for occlusal lesions that penetrate beyond the dentinal-enamel junction (DEJ).

2. MATERIALS AND METHODS

2.1 Sample Preparation

Teeth with no identifiers were collected from patients in the San Francisco Bay area and Geneva Switzerland with approval from the UCSF Committee on Human Research. Extracted teeth (n=120) were selected with occlusal and approximal lesions for this study. Teeth were sterilized using gamma radiation and stored in 0.1% thymol solution to maintain tissue hydration and prevent bacterial growth. Then, samples were mounted in black

orthodontic acrylic blocks from Great Lakes Orthodontics (Tonawanda, NY) and imaged with digital radiographs using a CareStream 2200 System from Kodak (Rochester, NY) operating at 60 kV.

All teeth were imaged using Microcomputed X-ray tomography (μCT) with a 10-μm resolution. A Scanco μCT 50 from Scanco USA (Wayne, PA) located at the UCSF Bone Imaging Core Facility was used to acquire the images. Visible color images of the samples were acquired using a USB microscope, Model AM7915MZT from AnMO Electronics Corp. (New Taipei City, Taiwan) with extended depth of field and cross polarization. The digital microscope captures 5 mega-pixel (2,952 × 1,944) color images.

2.2 SWIR Image Acquisition and Analysis

The SWIR reflectance images were captured using a Model GA1280J (Sensors Unlimited, Princeton, NK) camera with a 1280 × 1024 pixel format, a 15 μm pixel pitch and a bit depth of 12-bit. Two 1 in diameter planoconvex antireflection coated lenses of 60 mm and 100 mm focal length along with an adjustable aperture were placed between the handpiece and the InGaAs camera to provide a field of view of 11 mm × 11 mm at the focus plane. A low-OH optical fiber of 1 mm diameter was used to deliver light from a 1604 nm superluminescent diode (SLD), Model ESL 1620–2111 from Exalos (Schlieren, Switzerland) with an output of 17 mW and a bandwidth of 46 nm. The intensity delivered to the tooth was 5 mW. The transillumination light is delivered through two 0.4 mm diameter low-OH optical fibers. A 1314 nm (BW) SLD, Model DL-CS3452A-FP 1620–2111 from Denselight (Singapore) with an output of 48 mW and a bandwidth of 33 nm was used as the source for transillumination. A 50/50 beamsplitter was used to deliver light to each arm for transillumination. The output intensity of each arm was set at 10 mw before entering the Teflon plugs. The system and optical probe is described in [17]. The samples were dried of excess water with an air nozzle for 30 seconds before each reflectance image was taken due to the elevated water absorption at 1600 nm. [4]. Image processing of the images was performed by custom scripts written using MATLAB from Mathworks (Natick, MA). The acquired 12-bit images (4096) were converted to 16-bit (65535) by multiplying by 16 and subtracting 1 to facilitate processing using MATLAB. The contrast was calculated for each lesion using the formula $(I_L - I_S)/I_L$ for reflectance images and $(I_S - I_L)/I_S$ for transillumination images, where I_L is the average intensity in the lesion area ROI, and I_S is the average intensity in the sound ROI [5]. MicroCT image analysis and lesion structural measurements were carried out using Dragonfly from ORS (Montreal, Canada).

2.3 Lesion Depth Model (Reflectance Imaging)

This occlusal imaging model utilizes the Beer-Lambert Law and the two imaging geometries shown in Fig. 1 for occlusal lesions and interproximal lesions, respectively. Most occlusal lesions that are severe enough to penetrate into dentin and require surgical intervention have the geometry shown in Fig 1A. We have shown in *in vitro* and *in vivo* studies that this geometry can be exploited to detect severe occlusal lesions that are not yet visible on radiographs in OCT and SWIR images [18, 19]. A similar approach can also be applied to interproximal lesions (Fig. 1B) that originate from the proximal surfaces, however this

approach requires a 2nd occlusal lesion that is visible on the occlusal surface to provide the measurement for I_{L1}.

Model parameters are shown in Fig. 1. The contrast of subsurface lesion areas is calculated as: $Css = \frac{I_{L2} - I_S}{I_{L2}}$ and the contrast of lesions on the surface is $Cs = \frac{I_{L1} - I_S}{I_{L1}}$. We assume that the ratio of the light incident and reflected from the lesion at the surface is similar to the ratio of the light incident and reflected at the subsurface lesion inside the enamel. This ratio is called A:

$$\frac{I_1}{I_2} \approx \frac{I_0}{I_{L1}} = A$$

I_1 is the attenuation of I_0 at depth z in enamel:

$$I_1 = I_0 e^{-\mu_E z}$$

Where μ_E is the attenuation coefficient of sound enamel at 1600 nm. Based on references [22, 23], we chose μ_E to be 1.5 cm^{-1} in our model.

According to ratio A, I_2 is then written as:

$$I_2 = \frac{I_1}{A} = \frac{I_0}{A} e^{-\mu_E z}$$

I_{L2} is thus:

$$I_{L2} = I_2 e^{-\mu_E z} = \frac{I_0}{A} e^{-2\mu_E z}$$

Substitute A again:

$$I_{L2} = I_0 \frac{I_{L1}}{I_0} e^{-2\mu_E z} = I_{L1} e^{-2\mu_E z}$$

Therefore, z can be estimated as:

$$Z_{est} = \frac{ln \frac{I_{L1}}{I_{L2}}}{2\mu_E}$$

I_{L1} and I_{L2}, the intensities of the surface and subsurface lesions can be directly extracted from reflectance images as shown in Fig. 2A for occlusal lesions. A similar approach can be applied to interproximal lesions as shown in Fig. 3 using a second occlusal lesion for I_{L1}. The depth z_{est} calculated by our model was then compared with actual depth z_{act} measured with microCT.

The assessment of the lesion depth for interproximal lesions is more straightforward since the depth penetration from the proximal surface can be directly viewed from the occlusal surface through the transparent enamel at both 1300 and 1600 nm. Length measurements on lesion depth and width were performed on reflectance and transillumination images separately and microCT was used for comparison as shown in Fig. 4.

3. RESULTS AND DISCUSSION

We identified 10 samples with “hidden” subsurface occlusal lesions and 8 samples with both interproximal lesions and occlusal surface lesions on the same tooth. With I_{L2} and I_{L1} directly measured in reflectance images, we calculated the model predicted lesion depth using $\mu_E = 1.5\ cm^{-1}$. The estimated lesion depth and the depth measured with microCT is plotted in Fig. 5. The slope of the theoretical curve and the measured curve are different suggesting that a different value of μ_E may be more appropriate, this may be due to surface scattering or the influence of multiple scattering. For higher lesion depths, we anticipate greater contributions from multiple scattering and greater deviation from the model. It is encouraging that the model is capable of distinguishing shallow lesions from deep lesions based on intensities alone which is valuable for differentiating those lesions that are shallow and confined to enamel and those that penetrate deeper into the dentin and are more likely to require surgical intervention. We plan to further investigate this approach with a larger sample size in the future.

Comparison of the depth and width measurements for interproximal lesions is more straightforward. Forty-nine teeth with interproximal lesions were selected. In transillumination mode, the interproximal lesion depths measured by the dual probe show very high correlation with those measured with microCT as shown in Figs. 7 A&B. Both the actual depth penetration and the depth to the dentin enamel junction (DEJ) measured with microCT are plotted in Figs. 6 & 7. SWIR imaging methods have limited contrast over dentin and it is only necessary to show that the lesion is severe enough to penetrate to the underlying dentin. There is high correlation between occlusal transillumination and microCT for the lesion depth and shifting the cutoff to the DEJ only slightly improves the correlation (0.823 vs 0.807). The correlation of the lesion depth measured using SWIR reflectance and microCT showed lower correlation than for transillumination. There is low but significant correlation ($P<0.05$) between reflectance and microCT for the lesion depth and shifting the cutoff to the DEJ only slightly improves the correlation (0.25 vs 0.19). This result was not anticipated since in our prior clinical studies SWIR reflectance measurements were more sensitive than SWIR proximal and occlusal transillumination in the detection of caries lesion on both occlusal and proximal surfaces. The high sensitivity of reflectance imaging makes it perform better at detecting lesion presence, however transillumination performs better at estimating the severity of the detected lesion if the lesion appears with sufficient contrast to be detected.

Interproximal lesion widths were also compared. The lesion depth is of greater interest since it shows the depth of penetration, however the lesion width is also useful because it can be used to estimate the overall size of the lesion and is valuable for making a more informed decision on whether surgical intervention is recommended. The lesion widths for

SWIR reflectance and occlusal transillumination are shown in Fig. 8. The correlation of the lesion width in occlusal transillumination was also higher than for reflectance compared to microCT (0.237 vs 0.052).

This study shows that a simple model applied to SWIR reflectance images can provide lesion depth information and further aid in differentiating shallow occlusal lesions from the more severe deeply penetrating lesions. In addition, this study showed that occlusal transillumination images at 1300 nm were more valuable in providing lesion depth and width information regarding interproximal lesions than reflectance images at 1600 nm even though the later method of imaging has shown a higher sensitivity in previous studies. This study further demonstrates the value of the simultaneous acquisition of SWIR occlusal transillumination and reflectance images.

ACKNOWLEDGEMENTS

The authors would like to acknowledge the contributions of Jacob Simon, Marwa Abdelaziz and Cynthia Darling and support from NIDCR/NIH grant R01-DE028295.

5. REFERENCES

[1]. Jones R, Huynh G, Jones G, and Fried D, “Near-infrared transillumination at 1310-nm for the imaging of early dental decay,” Optics Express, 11(18), 2259–65 (2003). [PubMed: 19466117]

[2]. Fried D, Featherstone JDB, Darling CL, Jones RS, Ngaotheppitak P, and Buehler CM, “Early Caries Imaging and Monitoring with Near-IR Light,” Dental Clinics of North America - Incipient and Hidden Caries, 49(4), 771–794 (2005).

[3]. Buhler C, Ngaotheppitak P, and Fried D, “Imaging of occlusal dental caries (decay) with near-IR light at 1310-nm,” Optics Express, 13(2), 573–82 (2005). [PubMed: 19488387]

[4]. Zakian C, Pretty I, and Ellwood R, “Near-infrared hyperspectral imaging of teeth for dental caries detection,” J Biomed Opt, 14(6), 064047–7 (2009). [PubMed: 20059285]

[5]. Amaechi BT, Owosho AA, and Fried D, “Fluorescence and Near-Infrared Light Transillumination,” Dent Clin North Am, 62(3), 435–452 (2018). [PubMed: 29903560]

[6]. Staninec M, Lee C, Darling CL, and Fried D, “In vivo near-IR imaging of approximal dental decay at 1,310 nm,” Lasers Surg Med, 42(4), 292–8 (2010). [PubMed: 20432277]

[7]. Jones G, Jones RS, and Fried D, “Transillumination of interproximal caries lesions with 830-nm light,” Lasers in Dentistry X. Proc SPIE Vol. 5313 17–22 (2004).

[8]. Jones RS, Huynh GD, Jones GC, and Fried D, “Near-IR Transillumination at 1310-nm for the Imaging of Early Dental Caries,” Optics Express, 11(18), 2259–2265 (2003). [PubMed: 19466117]

[9]. Hirasuna K, Fried D, and Darling CL, “Near-IR imaging of developmental defects in dental enamel.,” J Biomed Opt, 13(4), 044011:1–7 (2008).

[10]. Lee C, Lee D, Darling CL, and Fried D, “Nondestructive assessment of the severity of occlusal caries lesions with near-infrared imaging at 1310 nm,” J Biomed Opt, 15(4), 047011 (2010). [PubMed: 20799842]

[11]. Karlsson L, Maia AMA, Kyotoku BBC, Tranaeus S, Gomes ASL, and Margulis W, “Near-infrared transillumination of teeth: measurement of a system performance,” J Biomed Opt, 15(3), 036001–8 (2010). [PubMed: 20615003]

[12]. Simon JC, Lucas SA, Lee RC, Staninec M, Tom H, Chan KH, Darling CL, and Fried D, “Near-IR Transillumination and Reflectance Imaging at 1300-nm and 1500–1700-nm for in vivo Caries Detection,” Lasers Surg Med, 48(6), 828–836 (2016). [PubMed: 27389018]

[13]. Lee C, Darling CL, and Fried D, “In vitro near-infrared imaging of occlusal dental caries using a germanium enhanced CMOS camera,” Lasers in Dentistry XVI. Proc SPIE Vol. 7549 0K:1–7 (2010).

[14]. Simon JC, Curtis DA, Darling CL, and Fried D, “Multispectral near-infrared reflectance and transillumination imaging of occlusal carious lesions: variations in lesion contrast with lesion depth,” Lasers in Dentistry XXIV. Proc. SPIE Vol. 10473 05:1–7 (2018).

[15]. Zhu Y, Chang N, Fried WA, Yang V, and Fried D, “A dual handheld SWIR transillumination/reflectance probe for imaging lesions on tooth occlusal and proximal surfaces,” Lasers in Dentistry XXVI. Proc. SPIE Vol. 11217 0J:1–7 (2018).

[16]. Zhu Y, Simon J, Ng C, and Fried D, “Compact in vivo handheld dual SWIR transillumination/reflectance imaging system for the detection of proximal and occlusal lesions,” Photonic Therapeutics and Diagnostics in Dentistry, Head and Neck Surgery, and Otolaryngology. Proc SPIE Vol.11627 0N:1–4 (2021).

[17]. Zhu Y, Abdelaziz M, Simon J, Le O, and Fried D, “Dual short wavelength infrared transillumination/reflectance mode imaging for caries detection,” J Biomed Opt, 26(4), (2021).

[18]. Staninec M, Douglas SM, Darling CL, Chan K, Kang H, Lee RC, and Fried D, “Nondestructive Clinical Assessment of Occlusal Caries Lesions using Near-IR Imaging Methods,” Lasers Surg Med, 43(10), 951–959 (2011). [PubMed: 22109697]

[19]. Simon JC, Kang H, Staninec M, Jang AT, Chan KH, Darling CL, Lee RC, and Fried D, “Near-IR and CP-OCT imaging of suspected occlusal caries lesions,” Lasers Surg Med, 49(3), 215–224 (2017). [PubMed: 28339115]

[20]. Ngaotheppitak P, Darling CL, and Fried D, “Measurement of the severity of natural smooth surface (interproximal) caries lesions with polarization sensitive optical coherence tomography,” Lasers Surg Med, 37(1), 78–88 (2005). [PubMed: 15889402]

[21]. Ngaotheppitak P, Darling CL, Fried D, Bush J, and Bell S, “PS-OCT of Occlusal and Interproximal Caries Lesions viewed from Occlusal Surfaces,” Lasers in Dentistry XII, Proc SPIE Vol.6137 0L 1–9 (2006).

[22]. Jones RS, and Fried D, “Attenuation of 1310-nm and 1550-nm Laser Light through Sound Dental Enamel,” Lasers in Dentistry VIII. Proc SPIE Vol. 4610 187–190 (2002).

[23]. Fried D, Glena RE, Featherstone JD, and Seka W, “Nature of light scattering in dental enamel and dentin at visible and near-infrared wavelengths,” Applied Opt, 34(7), 1278–85 (1995).

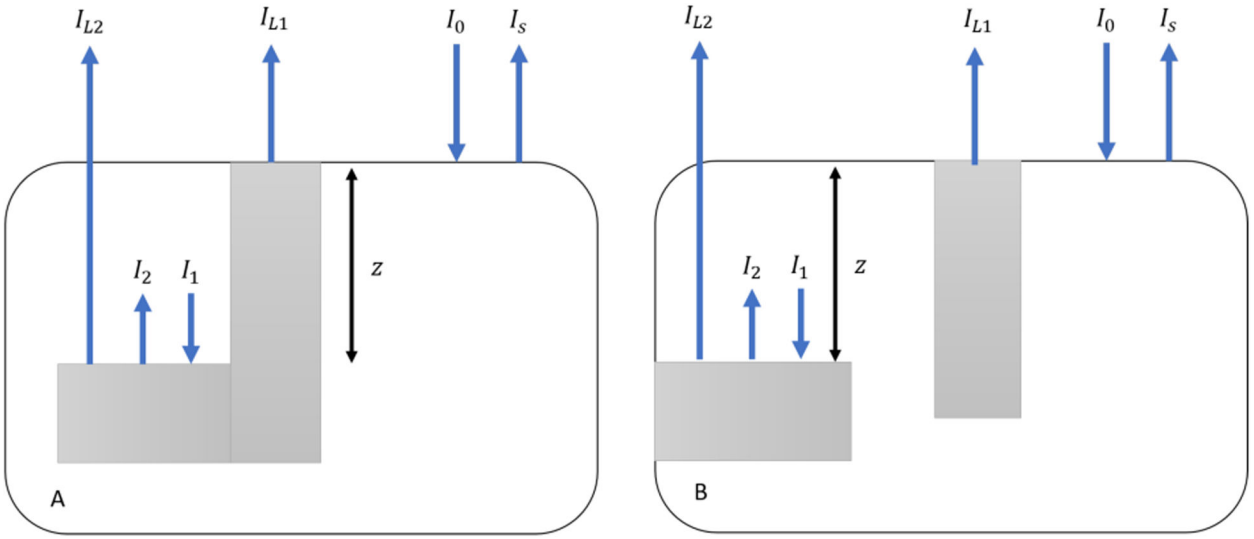

Fig. 1.

Models of occlusal (A) and interproximal (B) lesions viewed from the occlusal surface. White areas represent sound enamel and gray areas are lesion areas, respectively I_0 is the incident light intensity, I_S is the backscattered light from sound areas. I_{L1} is the backscattered light from lesion areas at the tooth surface. I_1 is the incident light and I_2 the backscattered light from the subsurface lesion areas. I_{L2} is light emitted from the tooth surface above subsurface lesion areas. Z is the distance of subsurface lesion areas below the tooth surface.

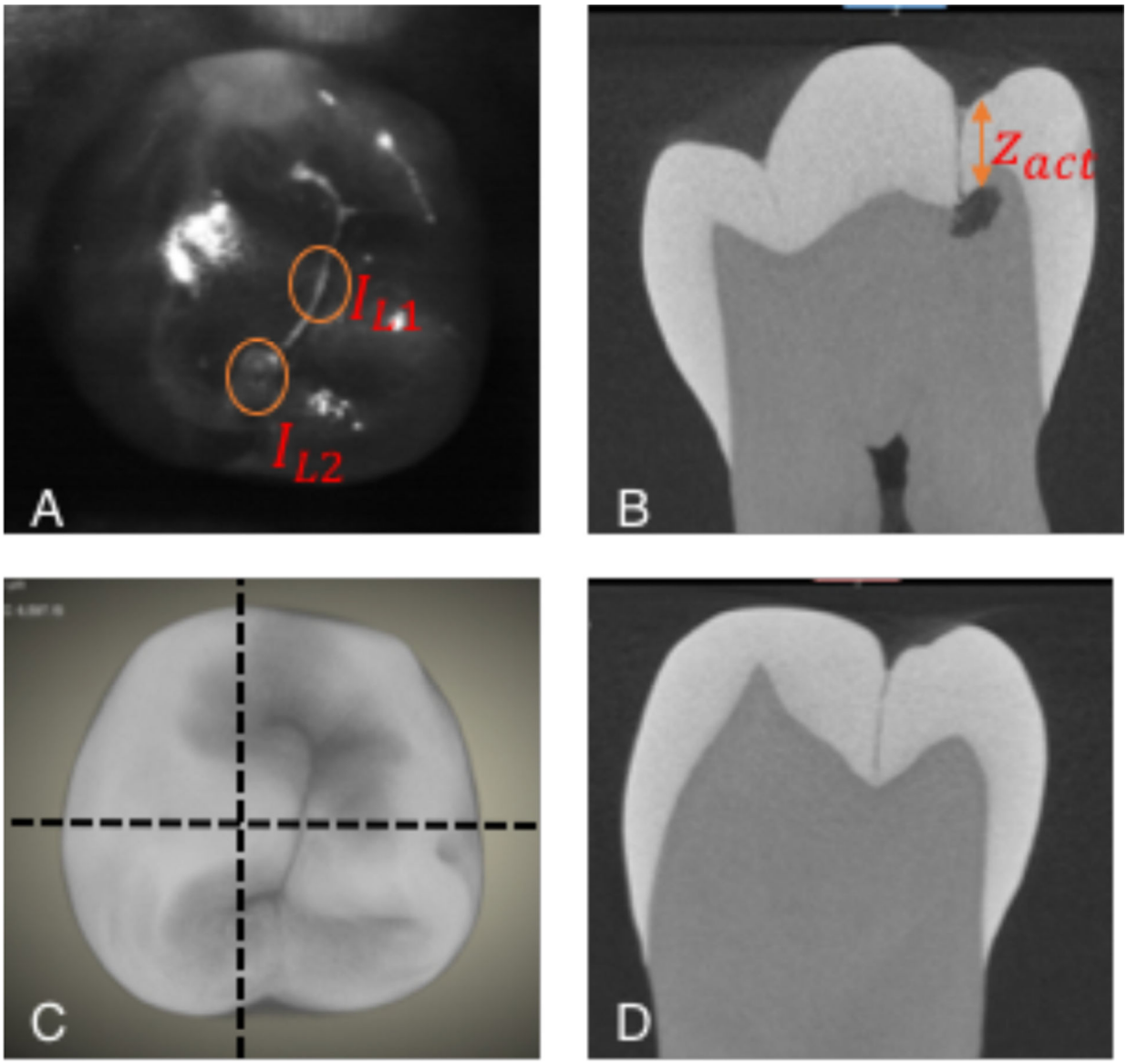

Fig 2.

(A) SWIR reflectance image of tooth occlusal surface showing positions of surface (I_{L1}) and subsurface lesion intensities (I_{L2}). (C) MicroCT 3D rendering of tooth's occlusal surface. Horizontal dashed lines show positions of cross sections in (B&D). The depth of the subsurface lesion z_{actual} is shown in (B).

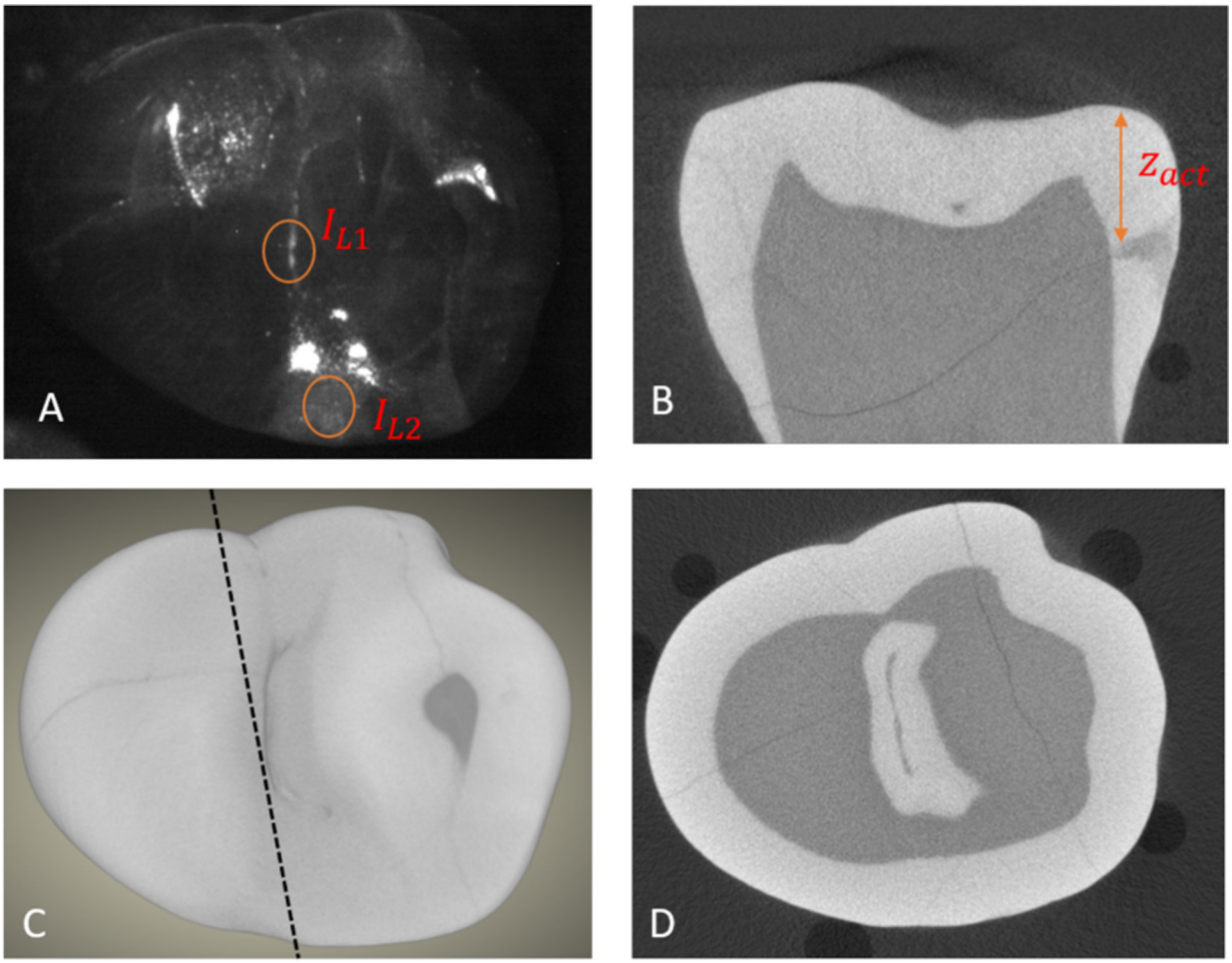

Fig. 3.

Estimating the depth from the occlusal surface of an interproximal lesion. (A) SWIR reflectance image of the tooth occlusal surface using a 2nd occlusal lesion for I_{L1} and the subsurface interproximal lesion intensity for I_{L2}. (C) MicroCT surface rendering, the dashed line shows the position of the extracted slice shown in (B) that shows the distance between the tooth surface and the interproximal lesion (z_{actual}). (D) MicroCT cross-section showing the occlusal surface lesion in the central fissure.

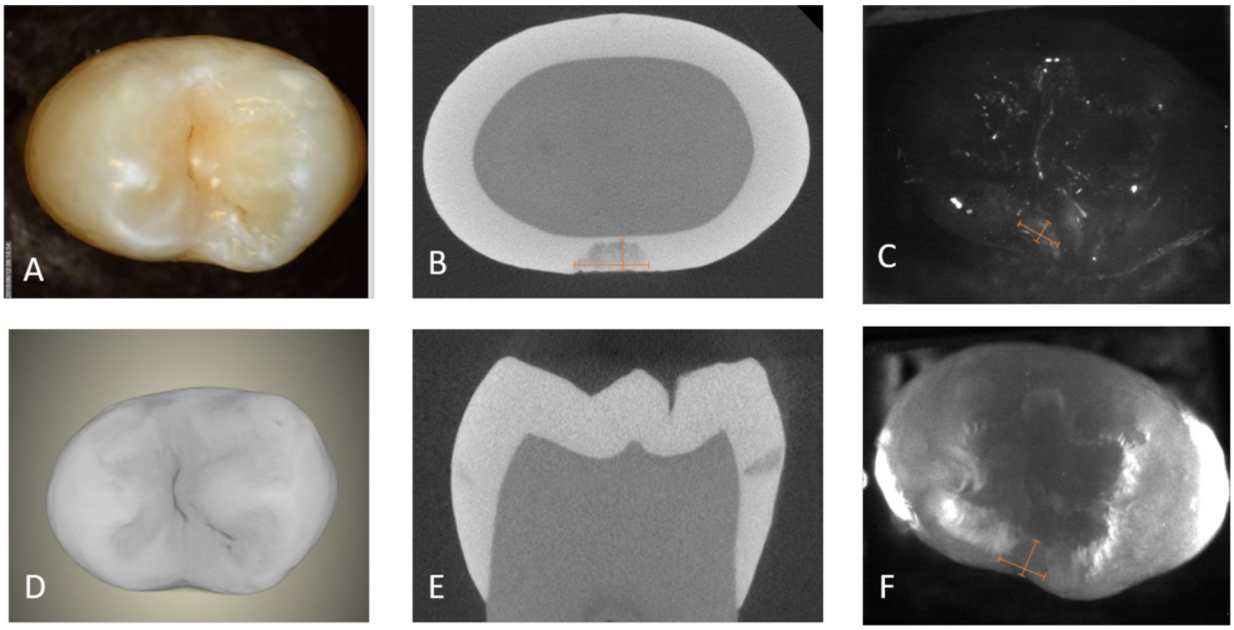

Fig. 4.

(A) color, (C) SWIR reflectance, (F) SWIR occlusal transillumination, and (D) MicroCT surface rendering with extracted slices in (B) and (E) showing the interproximal lesion and the depth and width measurements as shown by the two rulers in (B, C &F).

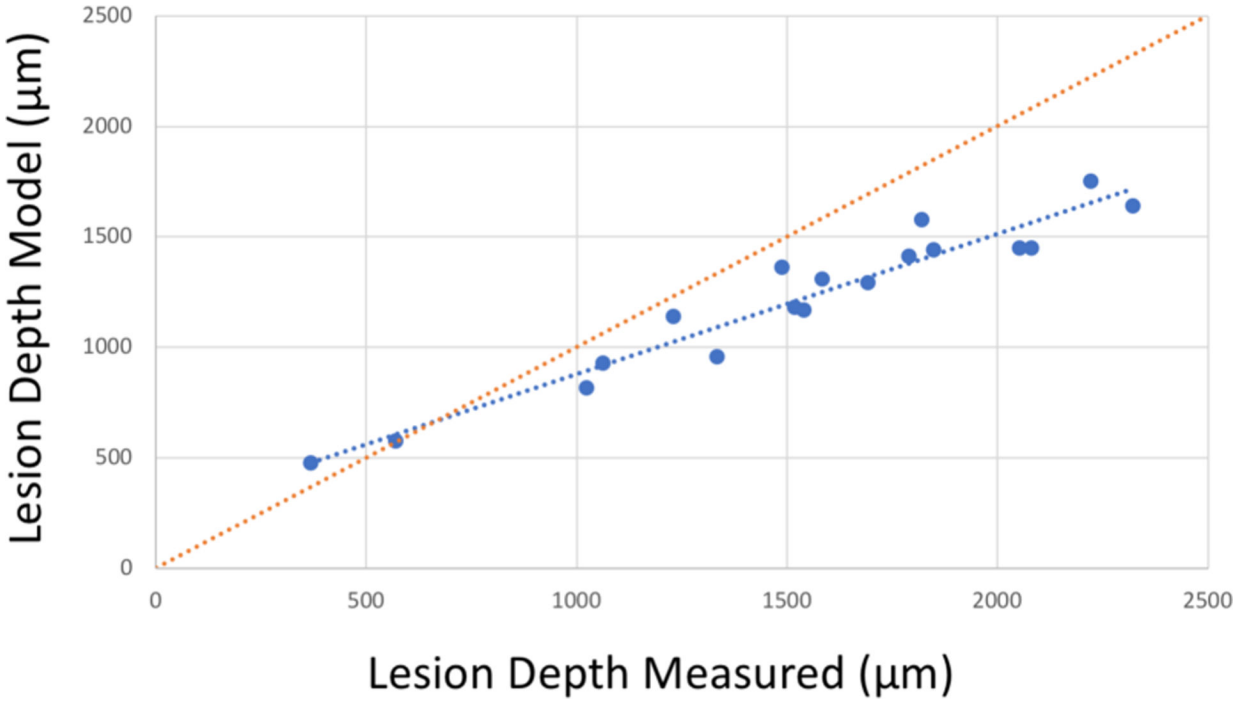

Fig. 5.

Model lesion depth estimated from SWIR reflectance vs. actual depth measured in microCT for “hidden” occlusal lesions and interproximal lesions with occlusal surface lesions as a reference point. The red dotted line represents matching depths for SWIR and microCT. There is high correlation of the lesion depth model with microCT (blue dotted line) R^2=0.93, P<0.05. The SWIR model underestimates the lesion depth for larger lesion depths.

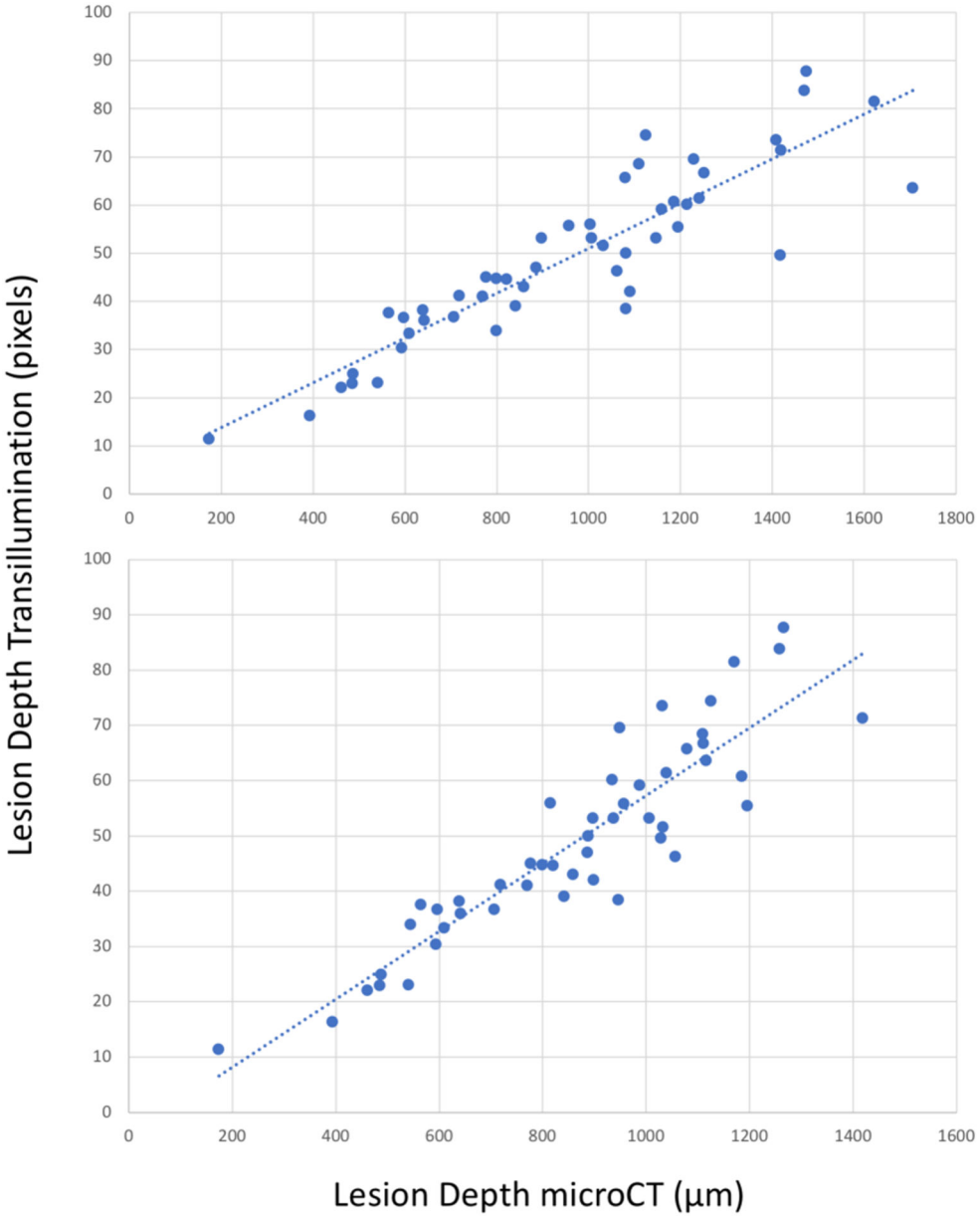

Fig. 6.

Interproximal lesion depth measured from the proximal surface in transillumination mode versus microCT. (top) Lesion depth measured with microCT and (bottom) cutoff at DEJ in microCT. There is high correlation with microCT (blue dotted lines) R^2=0.81 and 0.82 ($P<0.05$).

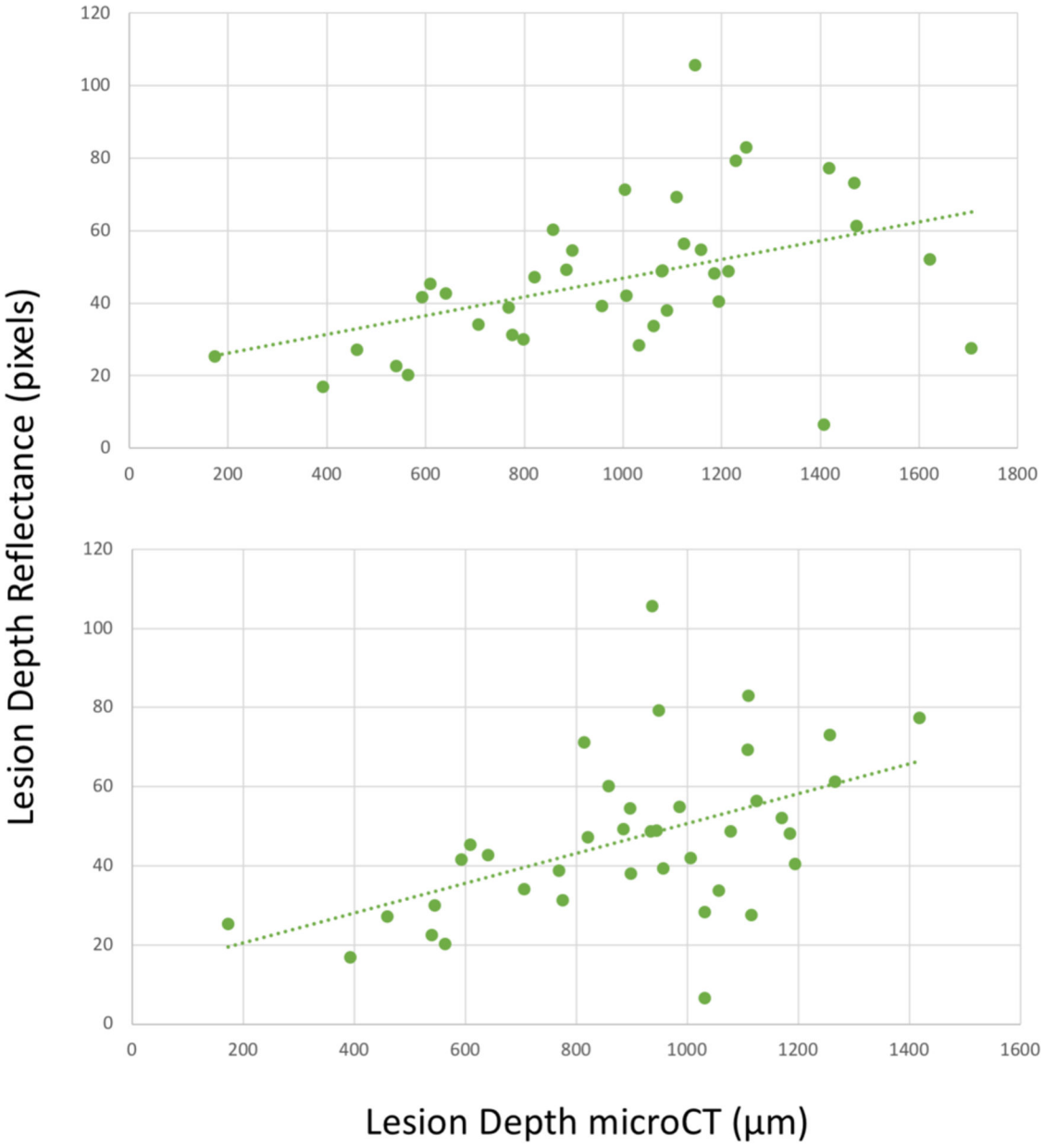

Fig. 7.

Interproximal lesion depth measured from the proximal surface in reflectance mode versus microCT measurement. (top) Actual lesion depth in microCT and (bottom) cutoff at the DEJ in microCT. There is correlation of the lesion depth with microCT (green dotted lines) R^2=0.19 and 0.25 ($P<0.05$).

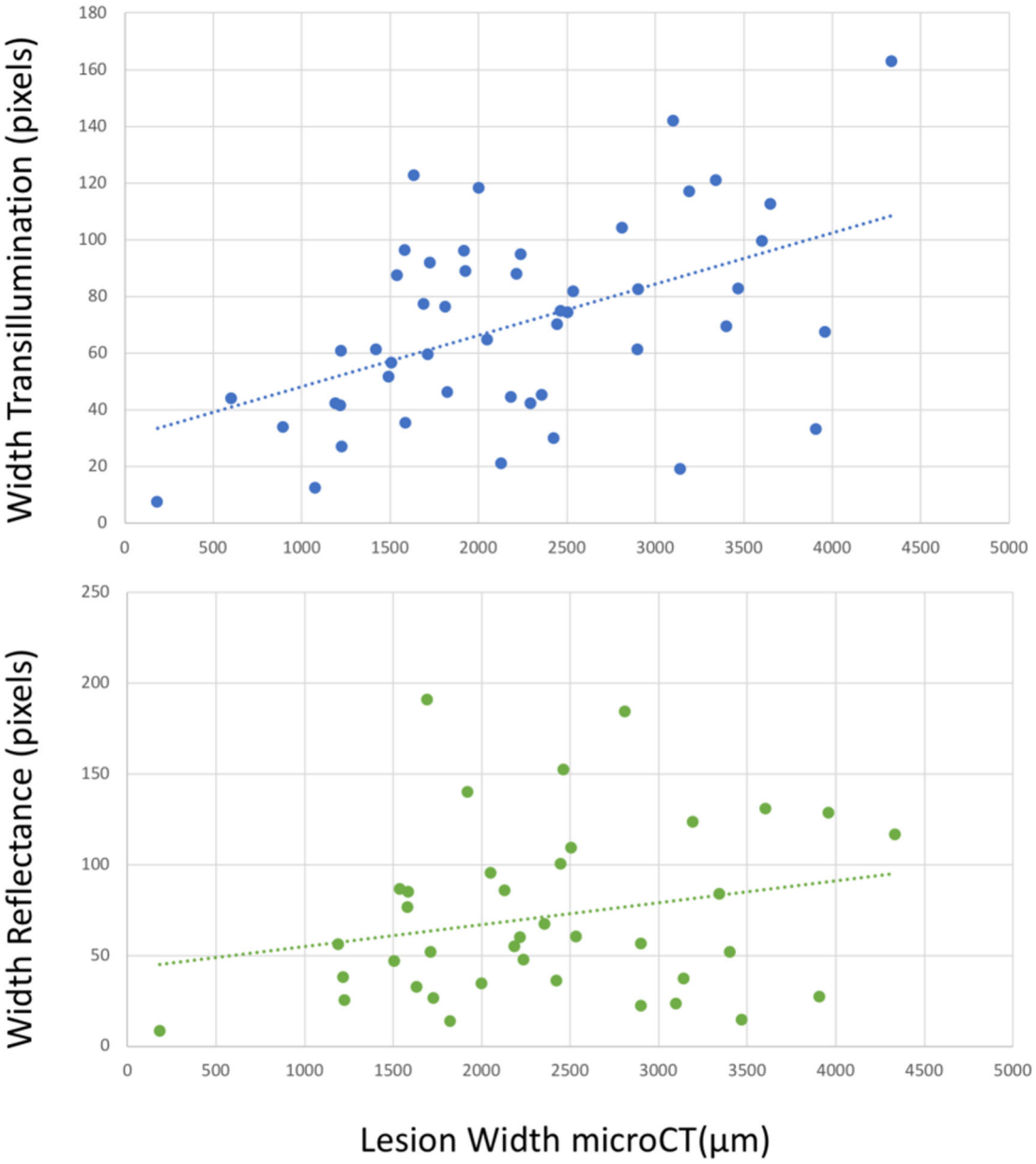

Fig. 8.

Interproximal lesion width measured from the proximal surface using reflectance and transillumination versus microCT. There is correlation of the lesion width measured with transillumination with microCT (blue dotted line) R^2=0.24, P<0.05 but not for reflectance (green dotted line) R^2=0.05, P>0.05.